2017

# Development of Ferroelectricity in the Smectic Phases of 4-Cyanoresorcinol Derived Achiral Bent-Core Liquid Crystals with Long Terminal Alkyl Chains

Sithara Pavithran Sreenilayam
*Dublin City University, Ireland*

J. K. Vij
*Trinity College Dublin, Ireland*

Yuri Panarin
*Technological University Dublin*, yuri.panarin@tudublin.ie

*See next page for additional authors*



## Recommended Citation

Sreenilayam, S.P., Vij, J. K. & Lehmann, A. (2017). Development of Ferroelectricity in the Smectic Phases of 4-Cyanoresorcinol Derived Achiral Bent-Core Liquid Crystals with Long Terminal Alkyl Chains. *Physical Review Materials, vol. 1, no. 3. doi:10.1103/PhysRevMaterials.1.035604*

# Development of ferroelectricity in the smectic phases of 4-cyanoresorcinol derived achiral bent-core liquid crystals with long terminal alkyl chains

S. P. Sreenilayam, Yu. P. Panarin, J. K. Vij, A. Lehmann, M. Poppe, and C. Tschierske

Phys. Rev. Materials **1**, 035604 — Published 16 August 2017

DOI: 10.1103/PhysRevMaterials.1.035604

# Development of ferroelectricity in the smectic phases of 4-cyanoresorcinol derived achiral bent core liquid crystals with long terminal alkyl chains

S. P. Sreenilayam[1], Yu. P. Panarin[1, 2], J. K. Vij[1*], A. Lehmann[3], M. Poppe[3], C. Tschierske[3]

[1]Department of Electronic and Electrical Engineering, Trinity College, The University of Dublin, Dublin 2, Ireland
[2]School of Electrical and Electronic Engineering, Dublin Institute of Technology, Dublin 8, Ireland
[3]Institute of Chemistry, Martin-Luther-University Halle-Wittenberg, Germany

Bent-core molecules can form numerous polar and symmetry broken liquid crystalline phases with fascinating properties. Here we report the characteristics of a new smectic phase, $SmC_SP_X$, found in the phase sequence of an achiral bent-core material with a 4-cyanoresorcinol bisbenzoate core, terminated by long linear alkyl chains (n=18) on both ends. This new phase exists over a narrow range of temperatures and is sandwiched in between the polar $SmC_SP_R$ and $SmC_SP_F$ phases with $\boldsymbol{P_S}$ ~ 250 nC/cm$^2$. In a planar-aligned cell it exhibits only chirality flipping on application of a conventional AC field but it also exhibits optical switching by rotation of the molecular directors on the tilt cone under a modified sequence of bipolar pulses. This changeover is discussed in terms of the model given by Nakata *et al.* (Phys. Rev. Lett. 96, 067802, 2006), involving a competition between the two forms of switching: the rotation around the long molecular axis and the switching through rotation of the molecular directors on the tilt cone. The model is modified to take account of the azimuthal pretilt and the molecular tilt angles. In addition to it, characteristics of a randomly polar synclinic smectic phase $SmC_SP_R$ are also discussed.

Email: jvij@.tcd.ie

## I. INTRODUCTION

Liquid crystals (LCs) characterized by fluidity and long-range order [1, 2] belong to a fascinating branch of soft condensed matter science. Bent-core LCs have recently been extensively investigated, these exhibit a large variety of phases with a set of unique properties. Some of the characteristics are: the polar order, the spontaneous breaking of the mirror symmetry and polar switching by electric fields. Bent-core LCs display a multitude of desirable properties while confined in cells with a thickness of the order of a few μm. Some of these characteristics form the basis of a range of applications currently being developed [3-12]. In

smectic phases of bent-core LCs, the mirror symmetry is broken by the orthogonal combination of tilt and polar direction and there exist different modes of correlations of tilt and polar direction in the neighboring layers. This in turn leads to a rich polymorphism of the polar smectic phases. These include orthogonal smectics where the plane formed by the long molecular axis and the polar director is parallel to the layer normal [13-21]. In most other smectic phases, the plane of the bent-core molecules is tilted to form smectic C (SmC) type phases, the tilt is either left or right from the layer normal and this leads to the formation of several additional sub-phases [22]. The main difference between the polar smectic phases of bent-core molecules (B2 phases) and the non-polar tilted smectic C (SmC) phase of normal rod-like molecules is that unlike the latter, different molecular configurations can exist among the neighboring layers with synclinic/ anticlinic molecular arrangements with respect to the tilt direction and syn-polar/ anti-polar with respect to the polarization vector. Furthermore these sub-phases exhibit ferroelectric (F) /antiferroelectric (A) properties. Their structures are described as: $SmC_SP_F$, $SmC_AP_A$, $SmC_SP_A$, and $SmC_AP_F$ [22] (Fig. 1), where $C_S$ stands for a synclinic and $C_A$ for an anticlinic tilt correlation in adjacent layers: $P_F$ and $P_A$ indicate the same and opposite directions of polar order in adjacent layers respectively.

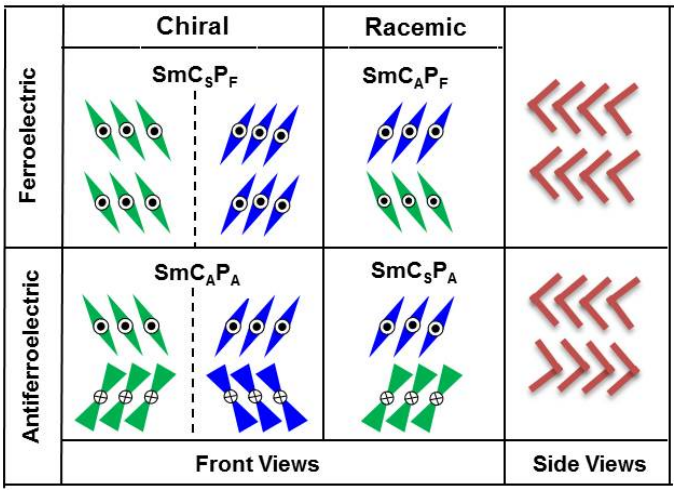


FIG. 1. Distinct views on the four subtypes of tilted polar smectic phases resulting from the correlation of the tilt and the polar directions (in the front views indicated by dots and crosses) of the bent-core molecules in adjacent layers [22]. The front views represent projections of bent-core molecules with the tip of the molecules in the direction 'in' or 'out' of the plane. The tip direction is coupled with the polar direction; dots and crosses indicate the polar direction pointing 'out' and 'into' the plane, respectively. An orthogonal combination of tilt and polar order leads to a reduced $C_{2v}$ symmetry and superstructural chirality of layers (color indicates chirality sense). The notations $P_A$ and $P_F$ refer to the antiferroelectric and ferroelectric polar order $C_A$ and $C_S$ refer to the anticlinic and synclinic tilt in adjacent layers. Ferro/antiferro arrangements have two chiral domains separated by a dashed vertical line on the left of this figure.

The bent-core molecules **1/n**, being reported here, consists of five aromatic rings with a central 4-cyanoresorcinol core. This bent 4-cyanoresorcinol core is connected with terephthalate based arms terminated by identical alkyl chains ($C_nH_{2n+1,}$ n=16,18) at both ends as shown in Fig. 2 [23]. A common feature of these 4-substituted resorcinols is the 'reduced bent angle' compared to the other bent-core mesogens without the 4-substituent [24]. In compounds **1/n**, the peripheral COO groups are reversed with respect to the previously reported series of 4-cyanoresorcinols involving 4-hydroxybenzoate rods, showing exclusively $N_{CybC}$ (cybotactic nematic phases composed of SmC clusters and SmC phases with larger tilt [25] compared to the compounds of the series **1/n**. This inversion of the peripheral COO groups leads to increased mesophase stability, enhanced polar order and the reduced tilt for compounds **1/n**. The lower tilt angle gives rise to unusual features and different characteristics, that result from a combination of reduced coherence length of the polar order and a weak inter-layer coupling. These special features lead to complex phase sequences with transitions between tilted and non-tilted phases. A strong influence of confinement and of sample history is found on the phases with different molecular arrangements [23, 26-29] and on the dependence of the induced tilt on the electric field [28].

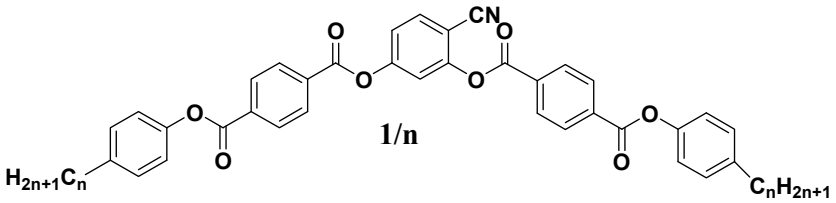


| Compd. | *T*/°C |
|---|---|
| **1/16** (n =16) | Cr 77 $SmC_AP_A$ 90 $SmC_SP_F^{hel}$ 110 $SmC_SP_R$ 125 SmA 162 Iso |
| **1/18** (n =18) | Cr 76 $SmC_AP_A$ 90 $SmC_SP_F$ / $SmC_SP_F^{hel}$ 110.2 $SmC_SP_X$ 110.7 $SmC_SP_R$134 SmA 160 Iso |

FIG. 2. Molecular structure of the investigated bent-core molecules; their mesophases and phase transition temperatures as observed on cooling from the isotropic liquid. Abbreviations: Iso = isotropic state, Cr = crystal; SmA = non-tilted and non-polar smectic phase, $SmC_SP_R$ = paraelectric smectic phase with uniform (synclinic) tilt and almost randomized polar direction of ferroelectric domains; $SmC_SP_F^{hel}$ = synclinic tilted ferroelectric smectic phase with a short pitch where the helical axis lies parallel to the layer normal; $SmC_AP_A$ = anticlinic tilted smectic phase with antiferroelectric polar order.

In this paper we focus specifically on the two compounds of the series **1/n** with longest alkyl chains, synthesized so far. Figure 2 lists the phase sequences and transition temperatures of the homologues with n = 16 and 18. In previous investigation of **1/16** and **1/18**, we focused on the spontaneous or field-induced development of a helical superstructure in $SmC_SP_F$ phase and the fast electro-optical switching [30]. Herein we investigate characteristics of a complete series of distinct paraelectric and polar smectic phases in more detail and thereby find a new phase

which appears only in a narrow temperature range, sandwiched in between the polarization randomized $SmC_SP_R$ and the polar $SmC_SP_F$ phases of compound **1/18**. The main focus of the present manuscript will be on this new phase tentatively designated as $SmC_SP_X$. We demonstrate switching of chirality in $SmC_SP_X$ phase by 'chirality flipping' as well as by rotation of the molecular director on the tilt cone depending on the form and the magnitude of the external electric field applied to the cell. In the $SmC_SP_R$ phase, both, polarization ***P*** and the permittivity $\Delta\varepsilon$, show critical behavior on approaching $SmC_SP_F$, similar to those exhibited by de-Vries smectics during the cooling process.

## II. EXPERIMENT

Experimental measurements are carried out on homeotropic and planar-aligned LC cells. Homeotropic alignment in a cell is obtained by coating the polymer AL60702 (JSR Korea) on the two ITO coated glass substrates. The substrates are baked at a temperature of 210 °C for 15 minutes each. A uniform polymer layer several 'nm' thick is adhered on to the substrate. ITO coating on the glass substrate that forms the bottom plate of the cell is etched to form two in-plane electrodes with a spacing of ~ 80 µm in between the two electrodes. An electric field at a frequency of 110 Hz is applied across these electrodes. Planar alignment in a cell is achieved by coating the substrates with RN1175 polymer (Nissan Chemicals Japan) and baking these at a temperature of 250 °C for 30 minutes. The cell thickness controlled by Mylar spacers is measured using an optical interference technique. The cell is mounted in a hot stage, fixed on to the rotating table of the polarizing optical microscope (Olympus BX 52). Temperature of the hot-stage is controlled by a Eurotherm 2604 temperature controller to an accuracy better than ± 0.05 $^{o}$C. To investigate the electro-optic behaviour of LC phases at higher fields, an electric signal from an Agilent 33120A signal generator amplified by a high voltage amplifier (TReK PZD700) is applied across the electrodes. Measurements of the dielectric permittivity and dielectric loss are made on a planar-aligned cell using a broadband Alpha High Resolution Dielectric Analyzer (Novocontrol GmbH, Germany) in the frequency range of 1 Hz - 10 MHz and by applying a weak electric field. Dielectric cells are made up of two ITO coated glass substrates with a planar-alignment layer on both substrates, and a low sheet resistance of the ITO layers, (20 Ω/□). A parastic capacitance of the cell containing the compound is in series with a low sheet resistance of the ITO electrodes. The product of R and C must ensure that the frequency of this arrangement is shifted beyond the desired experimental window of dielectric measurements.

## III. RESULTS AND DISCUSSION

### A. Polarizing optical microscopy and Electro-optical response study of compound 1/18

The texture of the SmA phase of **1/18** in a homeotropic cell (at T = 135.5 °C), formed on cooling the sample from the isotropic state is dark (Fig. 3a); this reflects uniaxiality of the phase. On reducing the temperature to 135 °C (Fig. 3b), parts of the cell show Schlieren texture. At 134.5 °C, a fully developed low-birefringent Schlieren texture is observed in a homeotropic cell (Fig. 3c), indicating that the transition to an optically biaxial mesophase has occurred. There is a striking pattern of equidistant stripes appearing across the developing Schlieren texture (Fig. 3b,c) which disappears on further cooling. This kind of stripe texture is typically observed for SmA-$SmA_b$ [31-33] and SmA to $SmC_A$ transitions [34-35]. This could indicate that that SmA-$SmC_SP_R$ transition occurs *via* an additional small range of an intermediate randomized $SmC_S$ domain structure with predominantly anticlinic tilt correlation betwee the domains [36] before this correlation becomes synclinic in the $SmC_SP_R$ range. However since an additional phase transition is not evident from other investigations (PM of planar samples, DSC, XRD, dielectrics), at the present state of knowledge it is considered as a kind of pre-or post-transitional phenomenon. A typical $SmC_S$ domain texture in a planar cell is recorded at a temperature of 113 $^oC$ (Fig. 3e). The textures show dark and bright areas (Figs. 3d and 3f) due to two tilt domains with director orientations being inclined at angles $\theta \approx \pm 18^o$ to the layer normal. In addition, four-brush disclination points are dominating in the Schlieren textures in homeotropic aligned cell (Fig. 4a). These observations show that the phase under discussion has a uniform molecular tilt in layers. The tilt is either left or right of the layer normal and thus forming distinct chiral domains belonging to a family of synclinic tilted smectic mesophases ($SmC_S$). When an electric field is applied across the planar aligned cell at a temperature of 113 °C (Fig. 3d-f and Fig. 6a, b (1)), the texture does not respond to the field, *i.e.* no optical switching occurs on the application of an electric field. As is typical for the $SmC_SP_R$ phase, chiral domains can be observed in homeotropic aligned cells [34]. The transition SmA-$SmC_SP_R$ is continuous and does not involve a measurable value of the transition enthalpy [30]. The $SmC_SP_R$ phase is often referred to as SmC because both phases possess the same $C_{2h}$ symmetry. Nevertheless, the physical characteristics of $SmC_SP_R$ and SmC phases are very different from each other. In contrast to the non-chiral SmC phase, the $SmC_SP_R$ phase shows properties related to polar phases. For example, a current response to an applied electric field is due to the polar switching, [30] and electric field induced polarization and soft mode like behavior of the tilt fluctuations are observed on approaching the polar SmCP-phases. Some of these observations follow from results of

dielectric measurements to be discussed later in the section on dielectric spectroscopy in section III C. Chiral domains are observed under certain conditions in homeotropic aligned cells (see Fig. 3g-i) which may indicate that phase biaxiality is not due to a restricted molecular rotation around their long molecular axes. It is more likely to be due to the tilt of the molecules, because only in this case layer chirality can develop.

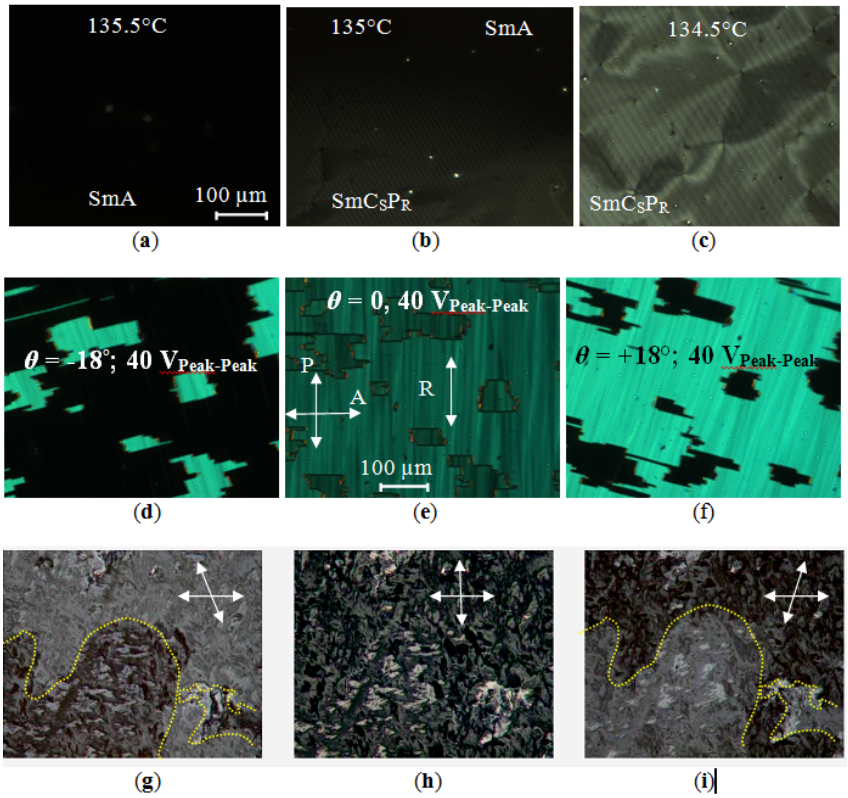


FIG. 3. (a-c) Polarizing micro-photographs of the SmA and $SmC_SP_R$ phases recorded under cooling in the absence of an external electric field in a homeotropic planar-aligned ITO cell of cell-thickness 6.5 µm filled with **1/18**. (d-f) $SmC_SP_R$ phase at 113 ºC in a 8 µm planar aligned cell; the textures are recorded by application of a 40 $V_{Peak-Peak}$ signal at a frequency of 110 Hz between the ITO coated electrodes; the rubbing direction ***R*** is (e) along the polarizer or is oriented at an angle $\theta$, (d) $\theta$ = -18° and (f) $\theta$ =+18° to the polarizer. (g - i) $SmC_SP_R$ phase at $T$ = 120°C in a homeotropic cell between ordinary glass plates showing chiral domains with opposite handedness, (h) between crossed polarizers, (g) and (i) with the polarizer rotated by 20° off the 90° position with respect to the analyzer, either in a clockwise or an anticlockwise direction; the brightness of domains is exchanged in (g) and (i), whereas rotation of the cell between the crossed polarizers does not lead to a change in the brightness; these observations indicate a conglomerate of chiral domains with opposite sign of optical rotation in the distinct domains.

The birefringence of the Schlieren texture continuously increases under cooling and this is clearly reflected in the visual textural changes. When an in-plane electric field at a frequency

of 110 Hz is applied at an amplitude of 10 V/µm in a homeotropic cell at a temperature of 113 °C, the initial Schlieren texture (Fig. 4a) transforms to a uniform one (Fig. 4c) and the birefringence increases with the field (Fig. 4d). On removal of the electric field, the high birefringent state (Fig. 4d) returns to a low birefringent one with Schlieren texture (Fig. 4a). This indicates that a field induced polar order parallel to the layer planes exists, and the electric field induced $SmC_SP_F$ state relaxes to the polarization randomized $SmC_SP_R$ one upon the removal of electric field.

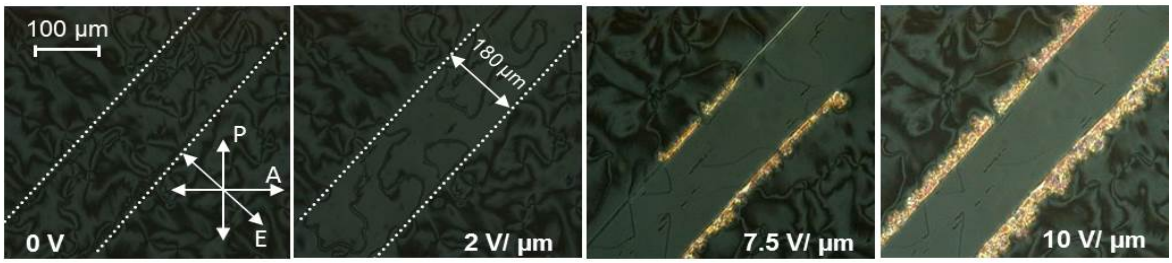


(a) (b) (c) (d)

FIG. 4. Polarizing optical microscopic textures of $SmC_SP_R$ phase of compound **1/18** at 113 ºC. (a - d) show the texures recorded in a 6.5 µm homeotropic aligned cell on the application of an in-plane electric field (*E*) at a frequency of 110 Hz, applied between the electrodes (the edges of electrodes are indicated by dashed white lines). The in-plane electrodes are fixed at an angle of 45º to the analyzer (A) / polarizer (P) as shown in (a). The distance between the two ITO electrodes is 180 µm.

On cooling the homeotropic cell below 113 °C the birefringence starts decreasing. The four brush Schlieren texture (Fig. 4a) at 113 °C slowly changes to a mosaic-like appearance (Fig. 5a, b) at temperatures of 111 °C and 110.8 °C, before reaching the optically uniaxial state (Fig. 5c) at 110.5 °C. On further cooling, the high temperature low biaxial phase ($SmC_SP_R$) transforms to a low temperature high biaxial $SmC_SP_F$ phase at 110.2 °C (Fig. 5d) and 110.0 °C (Fig. 5f).

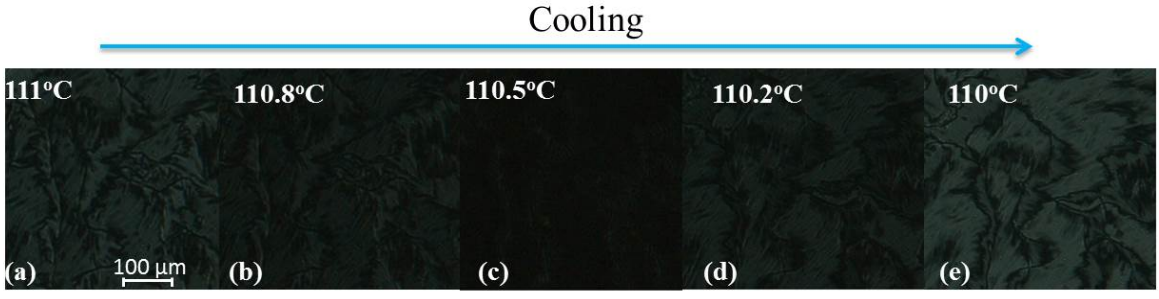

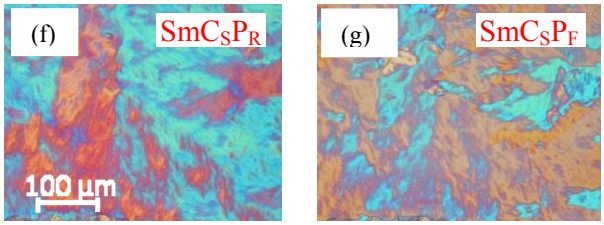


FIG. 5. Polarizing microphotographs of the LC phases of compound **1/18** in a homeotropic aligned cell ($d$=6 µm): (a) $SmC_SP_R$ at 111 ºC, (b) 110.8 ºC (c) $SmC_SP_X$ at 110.5 ºC (d), $SmC_SP_F$ at 110.2 ºC and (e) 110 ºC. Textures are recorded during the cooling process. To obtain textures (f) and (g) an additional λ-retarder plate is inserted in the homeotropic cell between the crossed polarizers at temperatures of (f) 120 °C and (g) at 100 °C, the last two figures indicate an inversion of birefringence.

The birefringence inversion is demonstrated by inserting an additional λ-retarder plate in between the crossed polarizers (see Figs. 5f, g). This inversion is due to the flipping of the secondary optical axis [29]. An appearance of the optical uniaxiality is considered as an indication of the formation of intermediate structure, provisionally labeled here as $SmC_SP_X$. The temperature range of this $SmC_SP_X$ phase is narrow and is restricted to lie only within ~ 0.5 ºC. For this reason, three structures corresponding to $SmC_SP_R$, $SmC_SP_X$ and $SmC_SP_F$ are observed simultaneously in a small temperature gradient cell (Fig. 6a, b at $U$ = 0 V). The sequence of structures is $SmC_SP_R$ (1), $SmC_SP_X$ (2) and $SmC_SP_F$ (3) as temperature decreases from the top to the bottom of the cell. The application of a conventional AC or DC voltage signal does not affect the textures in areas, (1) and (2), of the cell, corresponding to $SmC_SP_R$ and $SmC_SP_X$, respectively. On the other hand, in the $SmC_SP_X$ temperature range, an electric current flows on reversing the electric field which demonstrates electrical switching brought about by the field. A sudden reversal of the applied field causes reorientation of the polarization or polar vector around the long molecular axis (the so-called "chirality flipping" [35-38]) rather than the director switching on the tilt cone.

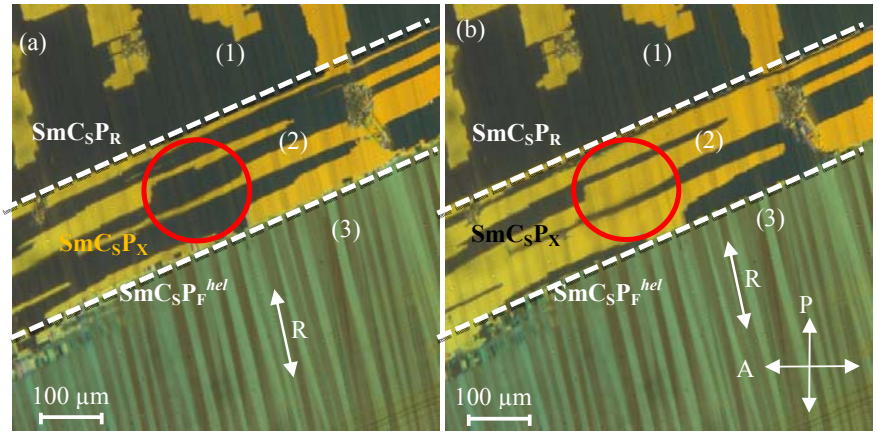


FIG. 6. Polarizing optical microscopic textures of the LC phases of compound **1/18** recorded in a small temperature gradient in a 8 µm planar aligned ITO coated cell in

between the two electrodes from higher temperature (top) to lower temperature (bottom): $SmC_SP_R$ (**1**) $SmC_SP_X$ (**2**) and $SmC_SP_F^{hel}$ (**3**). The cell is kept at a temperature of 110.5 ºC and the area (**2**) in (a) and (b) corresponds to $SmC_SP_X$ showing two bistable states, switched oppositely by reversing the polarity of the applied field via an intermediate short-circuited state, respectively. The red circle in (a) and (b) shows an aperture/area of the cell used for the electro-optical measurements. The white dashed lines in (a) and (b) separate out the $SmC_SP_R$, $SmC_SP_X$, and $SmC_SP_F^{hel}$ phases.

It must be stressed that the optical switching in the temperature range of $SmC_SP_X$ can be achieved only by reversing the polarity of the applied field through an intermediate state, short-circuiting of the electrodes of the cell (Fig. 6a→b; region 2). A reversal in the polarity through short-circuiting over a short period of 0.5 ms brings about both electrical and optical switching. The latter can only occur when the director rotates around the tilt cone. On the removal of the electric field, the optical texture returns to its previously switched state, thus showing bistability at $\boldsymbol{E} = 0$ (Fig. 6b→a; region 2). Such a phenomenon of optical and electric switching under special conditions has not so far been reported in the literature and is detailed below.

In order to investigate the electro-optical response of the sample in the $SmC_SP_X$ phase, a successful conduction of the experiment requires additional precautions to be observed since (i) the temperature range of this phase is quite narrow as stated previously, and (ii) the two opposite $\pm\theta$ domains coexist over an area smaller than the minimal aperture of the electro-optical set-up. Nevertheless, it is possible to select an area of the cell that corresponds to an almost single domain, as shown by red circles in Fig. 6a,b such that the average transmittance level over the aperture of Fig. 6a is less than that of Fig. 6b. Figure 7 shows a corresponding diagram to the oscilloscope screenshots that were recorded for the electro-optical response to the waveform of an applied voltage signal. As already stated, the $SmC_SP_X$ phase shows a polarization switching current but does not optically react to the square-wave signal except for the short spikes that appear on the polarity reversal, shown in Fig. 7a. On considering the importance of the short-circuited state of optical switching, we modify the applied voltage waveform by a sequence of bipolar square pulses separated by a zero-voltage signal existing over relatively short-times (*i.e.* short-circuit), $t_0$. Such a modified voltage waveform with a short-circuiting over a period of 0.5 ms causes the full electro-optical switching to occur. This waveform designed for the purpose is shown in Fig. 7b with 25 ms/div time scale and is expanded to a waveform of 1 ms/div shown in Fig.7c.

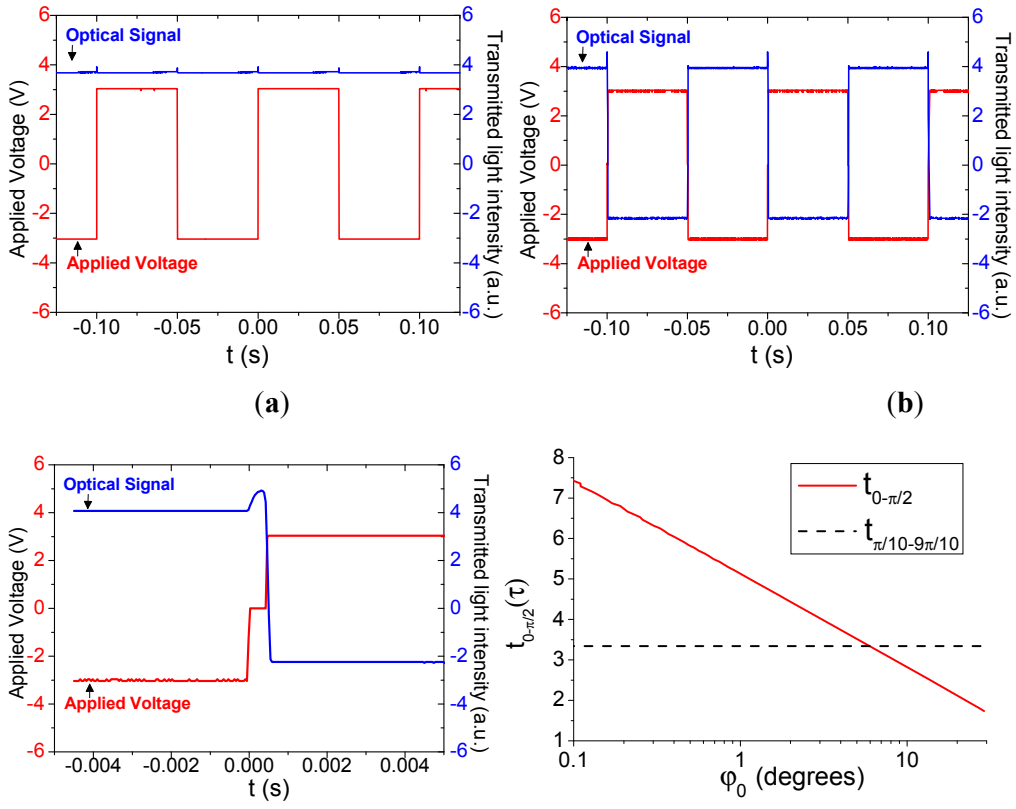


FIG. 7. Electro-optical response of a planar aligned 8 μm cell, filled with **1/18** in the $SmC_SP_X$ phase (T=110.5 °C), to different applied voltage waveforms (plots of the recorded oscilloscope screen-shots): (**a**) 60 V square-wave; (**b**) 60 V bipolar square pulses, separated by zero voltage over a time duration of 0.5 ms in between the pulses; (**c**) the same as (**b**) with time scale expanded to 1 ms/div, (**d**) the calculated dependence of the switching time on $\varphi$ from the initial $\varphi_0$ state to the critical π/2 state (solid red line) and from 10% π to 90% π (dashed black line) in the units of $\tau$, where $\tau$ is the time constant.

The switching dynamics was modelled theoretically in bent-core LCs in B1 [38] and B2 [39] phases. They consider two competing mechanisms of ferroelctric switching: (i) collective rotation around the long molecular axis, and (ii) collective rotation around the tilt cone. The EO response in B2 phases with temperature and electric field can satisfactorily be explained by Nakata et al.'s model [39] which considers two opposite chirality states separated by an energy barrier $U_{max}\cdot\cos^2(\beta)$. This model also considers two competing mechanisms of switching: (a) chirality flipping due to the molecular rotation around its long molecular axis by an angle $\beta$ and (b) the optical switching due to rotation of the molecular director on the tilt cone by an angle $\varphi$. The two dynamical states were modelled by a system of coupled differential equations. These are solved numerically using the Euler-Cauchy method [39]. A key feature of this solution is that both angles start changing from 0 to $\pi$ on the reversal of the applied electric field. The final switching achieved either by chirality flipping or by the optical switching depends on, which one

of the two angles, $\varphi$ or $\beta$, reaches the $\pi/2$ state first. When this angle has reached the $\pi/2$ state, this continues to grow to $\pi$, while the second one goes back to its initial value/state.

The experimental results show that for low electric fields (< *Ec*) the optical switching by φ-angle is observed. On an increase in the electric field greater than *E*c, the LC sample shows β-switching [35, 36, 39]. According to the model [39] the threshold field $E_C$ depends linearly on the energy barrier $U_{max}$. This model, however, does not explain explicitly the observed temperature dependence of the threshold field. This effect can be explained by the energy barrier $U_{max}$ depending on the molecular tilt angle, $\theta$ which in turn depends on temperature. Obviously it is zero for $\theta = 0$ and a maximum for $\theta = 90^o$, and the energy barrier can be expressed as $U_{max}=U_0 \cdot \sin^2\theta$. Therefore on an increase in temperature and a consequent decrease in the tilt angle, the energy barrier decreases with temperature. This assists the changeover to chirality flipping (β-switching). In $SmC_SP_X$ phase, the energy barrier is low enough to initially provoke 'chirality flipping', (due to a small tilt angle $\theta \approx 17^o$). However, the optical switching can also be achieved by using a specially designed sequence of pulses (as shown in Figs.7b and 7c) and by taking into account the azimuthal pretilt angle.

Earlier Xue et al. had discussed the switching of molecular directors on the cone in a ferroelectric SmC* phase consisting of chiral calamitic molecules. They derived analytical solution in *implicit* form, of time t in terms of $\varphi$(t), the azimuthal angle [40]. Valksman and Panarin, [41] solved it explicitly in terms of $\varphi(t)$ and from it, they found that the delay time $t_{0\text{-}10}$ (time taken by the response to go from its initial state of zero to reach 10% of the final response) depends strongly on the initial azimuthal (pretilt) angle $\varphi_0$, while the rise time $t_{10\text{-}90}$ (the time taken by the response to go from 10% to 90%) is independent of $\varphi_0$. In the simplest case of the dielectric anisotropy, measured at low frequencies, and specifically for $\Delta\varepsilon=0$, the dynamical equation has an exact analytical solution for $\varphi(t)$ [41]. The dependence of the switching of $\varphi$ from its initial state $\varphi_0$ to its critical π/2 state, $t_{\varphi 0 \text{ to } \varphi\pi/2} = \log(\pi/2/\tan(\varphi_0/2)) \approx \log(\pi/\varphi_0)$ was found. This is plotted in Fig. 7d as a function of $\varphi_0$. Based on such a solution, we consider two cases of optical response subjected to (i) a square□wave signal, and (ii) a series of bipolar pulses.

In the first case, the switching begins by reversing the polarity of the switched state. The switched state on the application of *E* makes the pretilt azimuthal angle $\varphi_0$ closer to zero due to large polar interactions of $\boldsymbol{P}$ with the field $\boldsymbol{E}$, ($\boldsymbol{P} \cdot \boldsymbol{E}$).This makes the delay time longer for switching by $\varphi$ (Fig. 7d) and the chirality flipping by $\beta$ is the only feasible outcome at this stage. In the second scenario, the optical switching by $\varphi$ begins when the electric field changes from a

finite value of $E$ to $E = 0$. In the latter case, the initial pre-tilt angle $\varphi_0$ grows from almost zero value to a finite value depending on the smectic layer tilt $\delta$ and the molecular tilt $\theta$ as

$\varphi_0 = sin^{-1}(tan(\delta)/tan(\theta))$ [42]. From this equation, value of $\varphi_0$ is found to range in between $10^o$ – $20°$ in the bookshelf structure depending on $\delta$ and $\theta$ but it takes a finite time for the relaxation to occur. The switching delay time (Fig. 7d) in this case from $\varphi_0$ to $\pi/2$, $t_{\varphi 0\text{-}\varphi\pi/2} \approx 2$ - 3 $\tau$. Here $\varphi$ will reach the critical value of $\pi/2$ prior to $\beta$ doing the same, the optical switching through $\varphi$ is then the outcome (Fig. 7b, c). Hence at the end of the negative pulse, the low initial value of $\varphi_0$ relaxes to a higher value at $E = 0$ but it takes a fraction of a millisecond to achieve (see the optical response at $E = 0$, Fig. 7c). When the duration for $E = 0$ is made longer than the relaxation time of $\varphi_0$ (~ 0.5 ms, for this case), the optical switching preferably occurs. However for shorter short-circuited time periods << 0.5 ms, the chirality flipping takes precedence and in that case chirality flipping is the only feasible outcome.

Summarizing, the POM and the electro-optical studies find that $SmC_SP_X$ is an intermediate uniaxial phase sandwiched in between the $SmC_SP_R$ and $SmC_SP_F$ phases and it has low enough energy barrier for chirality flipping and this occurs rather easily. But the optical switching can also be brought about by designing a special sequence of pulses applied to a planar-aligned cell and this has been demonstrated here.

## B. Birefringence ($\Delta n$) measurements

For carrying out the birefringence ($\Delta n$) measurements, the transmitted intensity from a well planar-aligned cell with good alignment is recorded. The rubbing direction ***R*** on the two substrates are made parallel to each other. ***R*** is fixed at an angle of $\alpha = 45°$ to the polarizer/analyser in a crossed polarizers system. The transmitted light ($T$) through a LC cell as a function of the effective birefringence ($\Delta n_{eff}$) is given by [43]:

$$T = A\sin^2\left(\frac{\pi\Delta n_{eff} d}{\lambda}\right) + B \qquad (1)$$

Here $\lambda$ is the wavelength, $d$ is the cell thickness. $A$ is the scaling factor and $B$ is the offset signal. The effective birefringence, $\Delta n_{eff}$, exhibits dispersion as a function of $\lambda$, the latter described by a modified Cauchy equation (2) [44,45].

$$\Delta n_{eff}(\lambda) = k_{eff}\left(\frac{\lambda^2\lambda^{*2}}{\lambda^2 - \lambda^{*2}}\right) \qquad (2)$$

$k_{eff}$ and $\lambda^*$ are the parameters of the Cauchy equation. Eqn. 2 is inserted in Eqn. 1 to take in account the optical dispersion. $k_{eff}$ and $\lambda^*$ are determined from fits of the transmitted spectrum at a particular temperature. $\lambda^*$ so determined is assumed to be a constant over the entire range of temperatures of investigation. The birefringence as a function of temperature is calculated from the transmittance spectra by using this determined value of $\lambda^*$. Figure 8 shows $\Delta n$, calculated as functions of temperature and voltage from the transmittance data of planar-aligned cells filled with the bent core LC materials **1/16** (a) and **1/18** (b) both as functions of temperature.

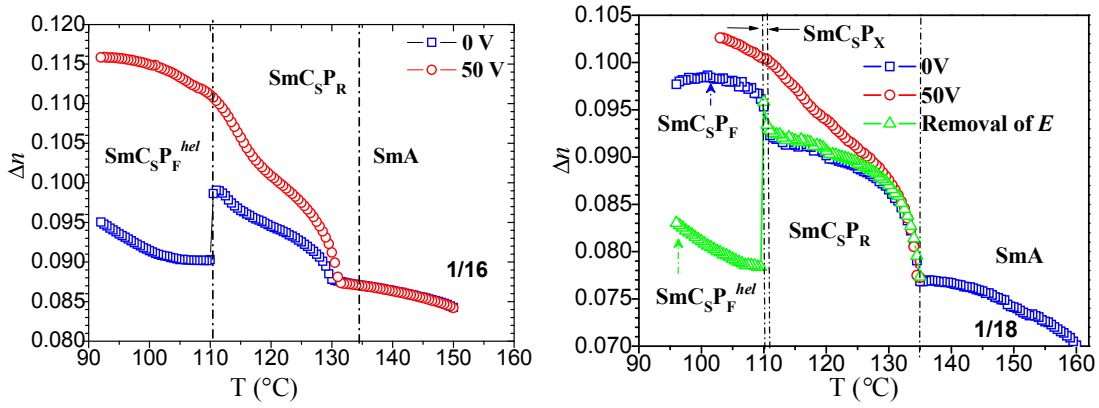


(a) (b)

FIG. 8. Temperature and the voltage dependencies of $\Delta n$ of the LCs (a) **1/16** and (b) **1/18**. The two substrates are rubbed parallel (***R*** on the cell substrates are parallel to each other). ***R*** is fixed at an angle of $\alpha$ = 45° to the crossed polarizer/analyzer directions. Measurements are carried out on planar-aligned cells under cooling for three different conditions: (i) a virgin state of the cell (□), (ii) under applied field (□) for both **1/16** and **1/18** and (iii) on the removal of the applied electric field (Δ) [green triangle symbol] for **1/18**.

The magnitude of $\Delta n$ increases on cooling from SmA to the SmC$_S$P$_F$ phase with characteristic jumps in $\Delta n$ occurring at each of the phase transition temperatures. Under a square wave voltage of 50 $V_{Peak\text{-}Peak}$ (f = 110 Hz), the magnitude of $\Delta n$, for both samples **1/16** and **1/18**, increases in the SmC$_S$P$_R$ and SmC$_S$P$_F$ phases. In the SmC$_S$P$_R$ phase, $\Delta n$ on removal of the electric field is almost equal to the magnitude prior to the field having been applied, for both compounds as in the textures recorded. In **1/16**, on further cooling from the SmC$_S$P$_R$ phase, a low birefringent state is observed and it increases with a decrease in temperature. This phase is assigned as 'helical SmC$_S$P$_F$' (SmC$_S$P$_F$$^{helical}$) with a very short helical pitch [30]. It is identical with the previously observed, but not fully investigated, helical SmCP$_\alpha$ phase found for the related compounds with alkoxy chains [29]. It is also related to the weakly tilted or non-tilted uniaxial smectic phase with helical rotation of the polar vector, observed for a shorter homologue of the series **1/n** with **n = 14** (also known as PAL 30). In that case, it had been designated as SmAPα, because the tilt was not measureable [17]. The observed low values of

birefringence in a planar-aligned cell [Figs. 8a, b] arise from the helical structure that gives rise to a 'uniaxial homeotropic texture' [30]. In the $SmC_SP_R$ and $SmC_SP_X$ phases of **1/18** the magnitude of $\Delta n$ on removal of the electric field is almost equal to its magnitude prior to the application of the field. In the $SmC_SP_F$ phase of **1/18**, the $\Delta n$ values after removal of the field are much lower than $\Delta n$ measured prior to the application of the field, in line with the formation of a helix in $SmC_SP_F$ after the cell has been treated by the electric field. This can be due to the field-induced weakening/breaking of the synclinic smectic inter-layer molecular interactions, which turn out to be stronger in the $SmC_SP_F$ phase of **1/18** (tilt, 23°) than in the same phase of **1/16** (with a smaller tilt, 17°). For the latter, the helix is spontaneously formed at the transition to the polar phase, whereas for **1/18** the polar smectic phase requires electric field treatment and in consequence the helical structure is induced in the latter. The helical state once formed/induced is retained even after the field has been removed. This implies that the $SmC_SP_F$ phase of **1/18** on transition from $SmC_SP_X$ temporarily retains a quasi-stable (surface stabilized) non-helical, uniformly polar structure which then transforms to the thermodynamically stable helical state with a short helical pitch. Once formed the helical state of $SmC_SP_F$ does not return or relax back to its initial uniformly polar $SmC_SP_F$ state.

The helical state arises as a consequence of the minimization of the electrostatic energy from a large in-layers spontaneous polarization $\boldsymbol{P}_S$ in the $SmC_SP_F$ phase. According to a simple phenomenological theory given by Pikin and Indenbom [46], the helical structure in tilted smectics is formed by a large spontaneous polarization and is independent of chirality. The latter determines the sense of the helical winding. For non-chiral LCs, formation of a helical structure reduces the electrostatic energy but at the same timr it increases the elastic energy. Stabilization of a helical structure is thus a compromise in between these two competing energies: electrostatic and elastic. The helical pitch is expressed as [46]:

$$p_0 = \frac{2\pi K\theta}{\mu P_S} \qquad (3)$$

where, $K$ is elastic constant, $\mu$ is the flexoelectric coefficient, $\theta$ is the tilt angle and $P_S$ is the spontaneous polarisation. The relatively small molecular bend angle in the polar smectic phases of compound **1/18** provides a weak polar coupling between the layers e.g. a lower elastic constant $K$. Therefore, in weakly tilted and weakly coupled polar smectics with large polarization (~400 nC/cm$^2$) the ratio $K/\boldsymbol{P_S}$ is very low when compared to the conventional SmC* phase of chiral calamitic molecules. This explains the existence of an anomalously short helical pitch (~15 nm) in **1/18** determined using Atomic Force Mocroscopy (AFM) [30].

## C. Dielectric spectroscopy

The complex permittivity $\varepsilon^* = \varepsilon' - i\varepsilon''$; ($i$ is the imaginary number) is measured as a function of frequency and temperature by applying a weak probe electric field to a planar-aligned cell. The experimental values of the dielectric strength ($\Delta\varepsilon$) and the relaxation frequency ($f_R$) are obtained for samples, **1/16** and **1/18**, by fitting the experimental dielectric spectra to the Havriliak-Negami equation [47],

$$\varepsilon^*(\omega) = \varepsilon' - i\varepsilon'' = \varepsilon_\infty + \sum_{j=1}^{n} \frac{\Delta\varepsilon_i}{\left[1 + (i\omega\tau_j)^{\alpha_j}\right]^{\beta_j}} - \frac{i\sigma_{dc}}{\varepsilon_0\omega} \qquad (4)$$

where $\varepsilon_\infty$ is the high frequency dielectric permittivity, $j$ varies from 1 to $n$ (where $n$ is the number of relaxation process), $\omega = 2\pi f$ is the angular frequency, $\varepsilon_0$ is the permittivity of free space, $\tau_j$ is the relaxation time, $\Delta\varepsilon_j$ is the corresponding dielectric relaxation strength, $\alpha_j$ and $\beta_j$ are the respective symmetric and asymmetric broadening parameters corresponding to the $j^{th}$ process. $\sigma_{dc}/\varepsilon_0\omega$ is the contribution of dc conductivity to $\varepsilon''$. The relaxation frequency, $f_j$, of the $j^{th}$ process

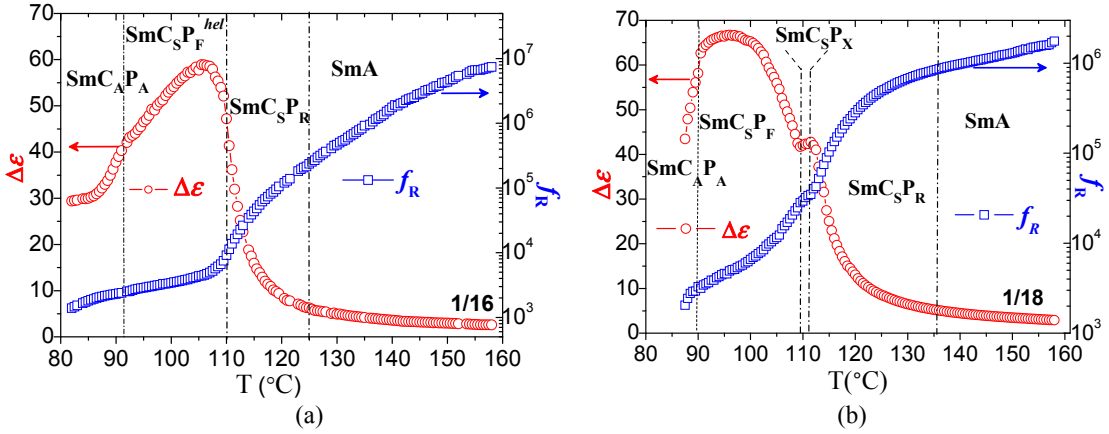


FIG. 9. Dielectric relaxation strength $\Delta\varepsilon$ (o) and corresponding relaxation frequency $f_R$ (□) for the two samples (a) **1/16** ($d$= 8 μm) and (b) **1/18** ($d$= 6.6 μm) in planar-aligned cells as a function of temperature. Meassurements are carried out under the cooling process.

is related to $\tau_j$ [48] as

$$f_j = \frac{1}{2\pi\tau_j}\left[\frac{\sin(\alpha_j\pi)}{2+2\beta_j}\right]^{1/\alpha_j}\left[\frac{\sin(\alpha_j\beta_j\pi)}{2+2\beta_j}\right]^{-1/\alpha_j} \qquad (5)$$

The temperature dependencies of $\Delta\varepsilon$ and $f_R$ for the main relaxation process are fitted to Eqn. 4, results from which are shown in Figs. 9a (**1/16**) and 9b (**1/18**) respectively.

The dielectric strength $\Delta\varepsilon$ of the SmC$_S$P$_R$ phase for both **1/16** and **1/18** samples increases gradually with decreasing temperature. This implies a soft mode-like increase in the correlations

of the neighboring molecules on transition to the polar SmCP phase. The corresponding $f_R$ of the relaxation process decreases with decreasing temperature. In the $SmC_SP_R$ phase close to the transition temperature of the $SmC_SP_F^{hel}$ (in **1/16**)/ $SmC_SP_F$ (in **1/18**) phase, the soft mode $\Delta\varepsilon$ sharply increases and $f_R$ sharply decreases. The temperature dependencies of $\Delta\varepsilon$ at the $SmC_SP_R$ to $SmC_SP_F$ are fitted to a power law equation $\Delta\varepsilon = k/(T-T_c)^{\gamma}$; exponent $\gamma$ is found as 1.5 for **1/16**, and 1.55 for **1/18**, both larger than the typical value of ~1.3 found for a conventional Sm*A* – Sm*C* phase transition. Magnitude of the exponent is reminiscent of the de Vries scenario at the Sm*A** to Sm*C** transition [49-51]. On further cooling of **1/18** in a planar-aligned cell, we observe a small step-like behavior in a narrow range of temperatures 110.7 ºC–110.2 ºC ($SmC_SP_X$) with a magnitude of $\Delta\varepsilon$ ~ 42.3 (Fig. 9b). However, in the **1/16** sample (Fig. 9a), $\Delta\varepsilon$ increases with a characteristic jump at the $SmC_SP_R$ to $SmC_SP_F^{hel}$ phase transition at 110 ºC and then decreases slowly on the formation of a helix. In the $SmC_SP_F^{hel}$ phase of **1/16** sample, the helix can easily be distorted by a weak external electric field and a change in the macroscopic polarization with the applied field is very significant and the relative permittivity is also large. The rise of $\Delta\varepsilon$ in the $SmC_SP_X$ and $SmC_SP_F$ phases of **1/18** can be explained by a competition between the increase in the polarization and a corresponding escape from the polar order through formation of a helical structure as well as forming anti-polar correlations on approaching the $SmC_AP_A$ phase. The latter is also composed of polar layers with polar directions alternating from layer to layer thus resulting in a decrease in $\Delta\varepsilon$. The dielectric behavior both in the dielectric strength and the relaxation frequency is characteristically different from the SmA* and SmC* phases of calamitic chiral LCs [52, 53].

## D. Polarization measurements

Figure 10 shows the temperature and field dependencies of the induced polarization ***P*** measured using planar-aligned cells, filled with compounds **1/16** and **1/18**. Measurements are carried out in the cooling process under application of a square voltage waveform of frequency 110 Hz using the method reported previously [41,42].

The shape of the polarization curves (Fig. 10a, b) as a function of temperature at electric fields up to 9 V/μm is similar to the observed temperature dependencies of dielectric strength $\Delta\varepsilon$ (Fig. 9a, b). In $SmC_SP_R$, both ***P*** and $\Delta\varepsilon$, show critical behavior similar to the de Vries Sm*A** to Sm*C** transition but different from the conventional Sm*A** to Sm*C** transition. In this phase, the measured polarization is electric field–induced and hence is field dependent. However, in the $SmC_SP_X$ (~250 nC $cm^{-2}$) and $SmC_SP_F$ phases of **1/18** and in the $SmC_SP_F^{hel}$ phase of **1/16** the ***P*** value is independent of the field, hence it is the spontaneous polarization. In the $SmC_AP_A$ phase ***P*** decreases for low electric fields (~390 nC $cm^{-2}$ at 80 ºC) due to the formation of

antiferroelectric order, while at higher electric fields, the ferroelectric state is induced and ***P*** grows to ~450 nC cm$^{-2}$.

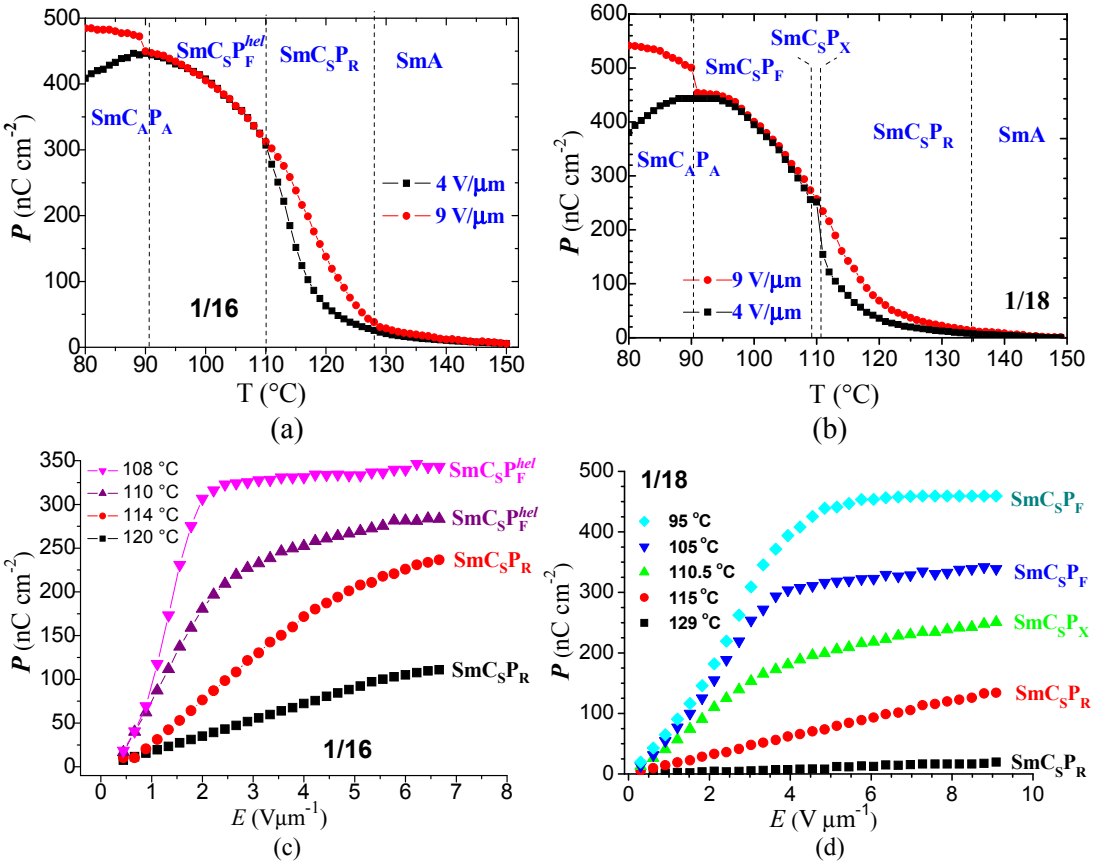


FIG. 10. Temperature and field dependencies of ***P*** measured in planar-aligned cells (a) and (c) filled with compound **1/16** (9 µm) and (b) and (d) filled with compound **1/18** (6.3 µm). Measurements are carried out by applying a square wave AC voltage waveform at a frequency of 110 Hz.

The field dependencies of ***P*** are shown in Fig. 10c, d. There is a linear increase with the field in the temperature range of $SmC_SP_R$ phase with its slope increasing with decreasing field, in line with that observed for paraelectric switching. In the $SmC_SP_F$ phase however, there is saturation at a field of 4 V µm$^{-1}$ followed by a plateau. These are the typical features of polar switching. In the intermediate state i.e in the $SmC_SP_X$ range of **1/18**, the field dependency of ***P*** is intermediate in between $SmC_SP_R$ and $SmC_SP_F$. In the temperature range of this phase an initial increasing trend in slope of ***P*** with temperature registers a decrease at ~ 4 Vµm$^{-1}$ but up to ~ 9 Vµm$^{-1}$ the ***P*** (***E***) curve does not appear to reach a plateau in ***P***.

## IV. CONCLUSIONS

A detailed investigation of 4-cyanoresorcinol bisbenzoate bent-core LCs terminated by long alkyl chains, n =**16**, **18** has been carried out by using a range of experimental methods: such

as polarizing microscopy, electro-optics, birefringence, dielectric and polarization measurements. Here we present results of a new intermediate $SmC_SP_X$ phase in **1/18** material at the transition from the short to the long-range polar order in the layers. This phase is an intermediate state in the transition in between $SmC_SP_R$ and $SmC_SP_F$ and is uniaxial with a low energy barrier for chirality flipping. Due to such a low barrier, the application of an electric field enables chirality flipping to occur, rather than electro-optical switching on the tilt cone, as observed for the majority of other polar smectic phases. Nevertheless, the $SmC_SP_X$ phase also shows optical switching on application of bipolar pulses separated by short-circuited pulses. This transition from chirality flipping to optical switching is explained by the dynamic model given by Nakata *et al.* [39] where additionally the initial pre-tilt angle, $\varphi_0$, is taken into account. The energy barrier depending on the molecular tilt angle is also taken into consideration. Switching by rotation of the director on a tilt cone is a signature of the transition from the Langevin-type switching in $SmC_SP_R$ to the polar optical switching in $SmC_SP_F$.

**Acknowledgements**

Work was initiated under the EU – FP7 – 216025 and finished off by 13/US/I2866 from the Science Foundation of Ireland as part of the US–Ireland Research and Development Partnership program jointly administered with the United States National Science Foundation under grant number NSF-DMR-1410649.

**References**

[1] P. G. de Gennes and J. Prost, The Physics of Liquid Crystals, (Clarendon, Oxford, 1993).

[2] S. Chandrasekhar, Liquid Crystals, (Cambridge University Press 1992).

[3] R. A. Reddy and C. Tschierske, J. Mater. Chem. **16**, 907 (2006).

[4] H. Takezoe and Y. Takanishi, Jpn. J. Appl. Phys. **45**, 597 (2006).

[5] T. Sekine, T. Niori, J. Watanabe, T. Furukawa, S. W. Choi and H. Takezoe, J. Mater. Chem. **7**, 1307 (1997).

[6] T. Niori, T. Sekine, J. Watanabe, T. Furukawa and H. Takezoe, J. Mater. Chem. **6**, 1231 (1996).

[7] S. P. Sreenilayam, Y. P. Panarin, J. K. Vij, M. Osipov, A. Lehmann, and C. Tschierske, Phys. Rev. E **88**, 012504 (2013).

[8] S. P. Sreenilayam, Y. P. Panarin, J. K. Vij, S. I. Torgova, A. Lehmann, and C. Tschierske, Phys. Rev. E **92**, 022502 (2015).

[9] E. Westphal, H. Gallardo, G. F. Caramori, N. Sebastian, M- G. Tamba, A. Eremin, S. Kawauchi, M. Prehm and, C. Tschierske, Chem. Eur. J. **22**, 8181 (2016).

[10] J. Etxebarria and M. B. Ros, J. Mater. Chem. **18**, 2919 (2008).

[11] R. A. Callahan, D. C. Coffey, D. Chen, N. A. Clark, G. Rumbles and D. M. Walba, ACS - Appl. Mater. Interfaces **6**, 4823 (2014).

[12] W. Iglesias and A. Jákli, in Handbook of Liquid Crystals, Vol. 8 (Eds. J. W. Goodby, P. J. Collings, T. Kato, C. Tschierske, H. F. Gleeson, P. Raynes), 2nd Ed., Wiley-VCH, Weinheim, pp. 799–817 (2014).

[13] A. Eremin, S. Diele, G. Pelzl, H. Nádasi, W. Weissflog, J. Salfetnikova, and H. Kresse, Phys. Rev. E **64**, 051707 (2001).

[14] B. K. Sadashiva, R. A. Reddy, R. Pratibha, and N. V. Madhusudana, J. Mater. Chem. **12**, 943 (2002).

[15] D. Pociecha, M. C□epic□, E. Gorecka, and J. Mieczkowski, Phys. Rev. Lett. **91**, 185501 (2003).

[16] K. Gomola, L. Guo, D. Pociecha, F. Araoka, K. Ishikawa, and H. Takezoe, J. Mater. Chem. **20**, 7944, (2010).

[17] Y. P. Panarin, M. Nagaraj, S. Sreenilayam, J. K. Vij, A. Lehmann, and C. Tschierske, Phys. Rev. Lett. **107**, 247801 (2011).

[18] R. A. Reddy, Ch. Zhu, R. Shao, E. Körblova, T. Gong, Y. Shen, E. Garcia, M. A. Glaser, J. E. Maclennan, D. M. Walba, and N. A. Clark, Science **332**, 72 (2011).

[19] T. Akutagawa, Y. Matsunaga and K. Yasuhara, Liq. Cryst. **17**, 659 (1994).

[20] S. Sreenilayam, M. Nagaraj, Y. P. Panarin, J. K. Vij, A. Lehmann, and C. Tschierske, Mol. Cryst. Liq. Cryst. **553**, 133 (2012).

[21] M. J. O'Callaghan, M. D. Wand, C. M. Walker and M. Nakata, Appl. Phys. Lett. **85**, 6344 (2004).

[22] D. R. Link, G. Natale, R. Shao, J. E. Maclennan, N. A. Clark, E. Körblova, and D. M. Walba, Science **278**, 1924 (1997).

[23] C. Keith, M. Prehm, Yu. P. Panarin, J. K. Vij and C. Tschierske, Chem. Commun. **46**, 3702 (2010).

[24] I. Wirth, S. Diele, A. Eremin, G. Pelzl, S. Grande, L. Kovalenko, N. Pancenkoa and W. Weissflog, J. Mater. Chem. **11**, 1642 (2001).

[25] C. Keith, A. Lehmann, U. Baumeister, M. Prehm and C. Tschierske, Soft Matter **6**, 1704 (2010).

[26] A. A. S. Green, R. F. Shao, J. E. MacLennan, M. A. Glaser, N. A. Clark, and C. Tschierske, Investigating the rich phase sequence of PAL30, poster ILCC2016-661, Kent State University, Ohio, July 31 to August 5, (2016).

[27] E. I. Kats and V. V. Lebedev, C1-11 ILCC2016-3 Non-linear fluctuation effects in dynamics of freely suspended films, ILCC2016, electronic abstracts, Kent State University, Ohio, July 31 to August 5, (2016).

[28] H. Ocak, M. Poppe, B. Bilgin-Eran, G. Karanlik, M. Prehm, and C. Tschierske, Soft Matter **12**, 7405 (2016).

[29] M. Alaasar, M. Prehm, M. Poppe, M. Nagaraj, J. K. Vij, and C. Tschierske, Soft Matter **10**, 5003 (2014).

[30] S. P. Sreenilayam, Y. P. Panarin, J. K. Vij, A. Lehmann, M. Poppe, M. Prehm, and C. Tschierske, Nat. Comm. **7**, 11369 (2016).

[31] (a) T. Hegmann, J. Kain, S. Diele, G. Pelzl and C. Tschierske, Angew. Chem. Int. Ed. **40**, 887 (2001). (b) R. Prathibha, N. V. Madhusudana and B. K. Sadasiva, Euro. Phys. Lett. **89** 46001 (2007). (c) C. Y. Yelamaggad, I. S. Shashikala, V. P. Tamilenthi, D. S. S. Rao, G. G. Nair and S. K. Prasad, J. Mater. Chem. **18**, 2906 (2008).

[32] (a) S. Radhika, B. K. Sadasiva and R. Prathibha, Liq. Cryst. **37**, 417 (2010). (b) A. Yoshizawa, M. Kurauchi, Y. Kohama, H. Dewa, K. Yamamoto, I. Nishiyama, T. Yamamoto, J. Yamamooto and H. Yokoyama, Liq. Cryst. **33**, 611 (2006).

[33] D. Guzeller, H. Ocak, B. Bilgin-Eran, M. Prehm, C. Tschierske, J. Mater. Chem. C **3**, 4269 (2015).

[34] (a) M. Alaasar, M. Prehm, M. Nagaraj, J. K. Vij and C. Tschierske, Adv. Mater. **25**, 2186 (2013); (b) M. Alaasar, M. Prehm, K. May, A. Eremin and C. Tschierske, Adv. Funct. Mater. **24**, 1703 (2014).

[35] A. Eremin, S. Diele, G. Pelzl, and W. Weissflog, Phys. Rev. E **67**, 020702 (2003).

[36] M.W. Schröder, S. Diele, G. Pelzl and W. Weissflog, ChemPhysChem, **5**, 99 (2004).

[37] G. Pelzl, M.W. Schröder, A. Eremin, S. Diele, B. Das, S. Grande, H. Kresse, and W. Weisslog, EPJE, **21**, 293 (2006).

[38] E. Gorecka, N. Vaupotic□, D. Pociecha, M. C□epic□, and J. Mieczkowski, ChemPhysChem, **6**, 1018 (2005).

[39] M. Nakata, R.-F. Shao, J. E. Maclennan, W. Weissflog, and N. A. Clark, Phys. Rev. Lett. **96**, 067802 (2006).

[40] J. I. Xue, M. A. Handschy and N. A. Clark, Ferroelectrics **73**, 305 (1987).

[41] V. M. Vaksman, and Yu. P. Panarin, Mol. Mats. **1**, 147 (1992).

[42] Yu. P. Panarin, Yu. P. Kalmykov, S. T. Mac Lughadha, H. Xu and J. K. Vij, Phys. Rev .E **50**, 4763 (1994).; Yu. P. Panarin, H. Xu, S. T. Mac Lughadha, and J. K. Vij, Jap. J. Appl. Phys. **33**, 2648 (1994).

[43] O. E. Panarina, Yu. P. Panarin, F. Antonelli, J. K. Vij, M. Reihmann and G. Galli, J. Mater. Chem. **16**, 842 (2006).

[44] J. Li and S.-T. Wu, J. Appl. Phys. **95**, 896 (2004).

[45] S. P. Sreenilayam, V. P. Panov, J. K. Vij and G. Shanker, Liq. Cryst. **44**, 244 (2016).

[46] S. A. Pikin and V. L. Indenbom, Ferroelectrics **20**, 151 (1978).

[47] S. Havriliak, Jr. and S. Negami, Polymer **8**, 161 (1967).

[48] O. E. Kaliovskaya and J. K. Vij, J. Chem. Phys. **112**, 3262 (2000).

[49] A. de Vries, J. Chem. Phys. **71**, 25 (1979).

[50] U. Manna, J. -K. Song, G. Power, and J. K. Vij, Phys. Rev. E **78**, 021711 (2008).

[51] (a) S. P. Sreenilayam, D. M. Agra-Kooijman, V. P. Panov, V. Swaminathan, J. K. Vij, Yu. P. Panarin, A. Kocot, A. Panov, D. Rodriguez-Lojo, P. J. Stevenson, M. R. Fisch and S. Kumar, Phys. Rev. E **95**, 032701 (2017). (b) N. Yadav, V. P. Panov, V. Swaminathan, S. P. Sreenilayam, J. K. Vij, T. S. Perova, R. Dhar, A. Panov, D. Rodriguez-Lojo and P. J. Stevenson, Phys. Rev. E **95**, 062704 (2017).

[52] H. Xu, J. K. Vij, A. Rappaport, and N. A. Clark, Phys. Rev. Lett. **79**, 249 (1997).

[53] A. Kocot, R. Wrzalik, J. K. Vij, M. Brehmer, and R. Zentel, Phys. Rev. B **50**, 16346 (1994).